Preprint of the manuscript:

Automated shear-wave splitting analysis for single- and multi- layer anisotropic media

T.S. Hudson, J. Asplet, A.W. Walker

This manuscript is currently under evaluation in Seismica.

Automated shear-wave splitting analysis for single- and multi- layer anisotropic media

Thomas S. Hudson [*,1], **Joseph Asplet** [2], **Andrew M. Walker** [1]

[1]Department of Earth Sciences, University of Oxford, Oxford, UK, [2]School of Earth Sciences, University of Bristol, Bristol, UK

Author contributions: *Conceptualization*: T. Hudson. *Methodology*: T. Hudson, J. Asplet. *Software*: T. Hudson, A. Walker. *Formal Analysis*: T. Hudson, J. Asplet, A. Walker. *Writing - original draft*: T. Hudson.

Abstract Shear-wave velocity anisotropy is present throughout the earth. The strength and orientation of anisotropy can be observed by shear-wave splitting (birefringence) accumulated between earthquake sources and receivers. Seismic deployments are getting ever larger, increasing the number of earthquakes detected and the number of source-receiver pairs. Here, we present a new software package, SWSPy, that fully automates shear-wave splitting analysis, useful for large datasets. The software is written in python, so it can be easily integrated into existing workflows. Furthermore, seismic anisotropy studies typically make a single-layer approximation, but in this work we describe a new method for measuring anisotropy for multi-layered media, which is also implemented. We demonstrate the performance of SWSPy for a range of geological settings, from glaciers to Earth's mantle. We show how the package facilitates interpretation of an extensive dataset at a volcano, and how the new multi-layer method performs on synthetic and real-world data. The automated nature of SWSPy and the discrimination of multi-layer anisotropy will improve the quantification of seismic anisotropy, especially for tomographic applications. The method is also relevant for removing anisotropic effects, important for applications including full-waveform inversion and moment magnitude analysis.

1 Introduction

Shear-wave velocity anisotropy is present in various media on Earth, from the mantle to the crust and even near-surface structures such as the cryosphere (Crampin and Chastin, 2003; Savage, 1999; Harland et al., 2013). This anisotropy can be measured using the phenomenon of shear-wave splitting, or seismic birefringence (Crampin, 1981; Silver and Chan, 1991). As a shear-wave propagates through a transversely anisotropic medium, it splits into two quasi-shear-waves, the fast and slow shear-waves (see Figure 1). This anisotropy can be caused by multiple factors,

*Corresponding author: thomas.hudson@earth.ox.ac.uk

including crystallographic-preferred orientation and shape-preferred orientation anisotropy (Kendall, 2000). Shear-wave splitting can be used to measure the anisotropic orientation of the fabric fast-direction, with the strength of anisotropy quantified by the delay-time between the fast and slow shear-waves.

Shear-wave velocity anisotropy has various applications related to past and present strain and deformation. In the mantle, one can image shear and mineral transitions (Savage, 1999; Liptai et al., 2022; Wolf et al., 2022; Wookey and Kendall, 2008; Vinnik et al., 1998; Sicilia et al., 2008). In the crust, one can image the orientation of fractures at volcanoes (Savage et al., 2010; Johnson et al., 2011; Bacon et al., 2021; Nowacki et al., 2018; Hudson et al., 2023) and hydrocarbon or CO_2 storage reservoirs (Verdon and Kendall, 2011; Baird et al., 2017), for example. At Earth's surface, anisotropy can be used to infer the accumulation of strain and past deformation in ice streams (Harland et al., 2013; Smith et al., 2017; Kufner et al., 2023; Hudson et al., 2021) and crevasse fracture networks (Gajek et al., 2021). It is also useful to measure shear-wave velocity anisotropy since its effects may need to be compensated for. In full-waveform inversion, if anisotropy is either not adequately modelled or removed then it will not be possible to reconcile phase and amplitude misfit. Similarly, shear-wave splitting may result in spurious/ambiguous S-wave phase arrival time picks, affecting travel-time velocity results. The energy partitioning may also affect earthquake spectra measurements that are used for calculating earthquake moment release. Furthermore, the majority of studies to date assume a single effective layer of anisotropy. However, for many systems there may actually be a number of layers with different anisotropic properties. A means of measuring multi-layer anisotropy is important to more fully describe the physical properties of such systems or if one wishes to more comprehensively remove anisotropic effects.

Here, we describe SWSPy, a new, open-source software package for shear-wave splitting analysis. The package is implemented in python, so that it is familiar to a wide community of users, can easily be implemented into existing workflows, is straight forward to install, is parallelised, and can be deployed on High Performance Computing (HPC) architecture. SWSPy is specifically designed to be a fully automated method, which can process large seismic datasets of thousands of events at thousands of receivers. This is important since recent advances in seismic instrumentation and data storage now enable datasets comprising orders of magnitude more receivers to be deployed, reducing the magnitude of completeness with a corresponding increase in number of detected earthquakes. Although the package is implemented in python, the most computationally expensive component is compiled to maximise efficiency. SWSPy also supports a three-dimensional splitting measurement (using the coordinate system of Walsh et al., 2013) and can be applied to analyse shear-wave splitting for multi-layer scenarios. SWSPy therefore complements other existing semi-automated, single-layer shear-wave splitting packages (Wuestefeld et al., 2010; Savage et al., 2010; Mroczek et al., 2020; Spingos et al., 2020). In this study we describe the method and provide a set of examples evidencing the performance of the software.

2 Methods

Shear-wave splitting through an anisotropic medium with a single dominant fabric can be described by two parameters: the delay-time δt between the fast and slow S-wave arrivals; and ϕ, the direction of polarisation of the fast S-wave in the plane transverse to propagation (see Figure 2). Various methods exist for measuring these quantities, including

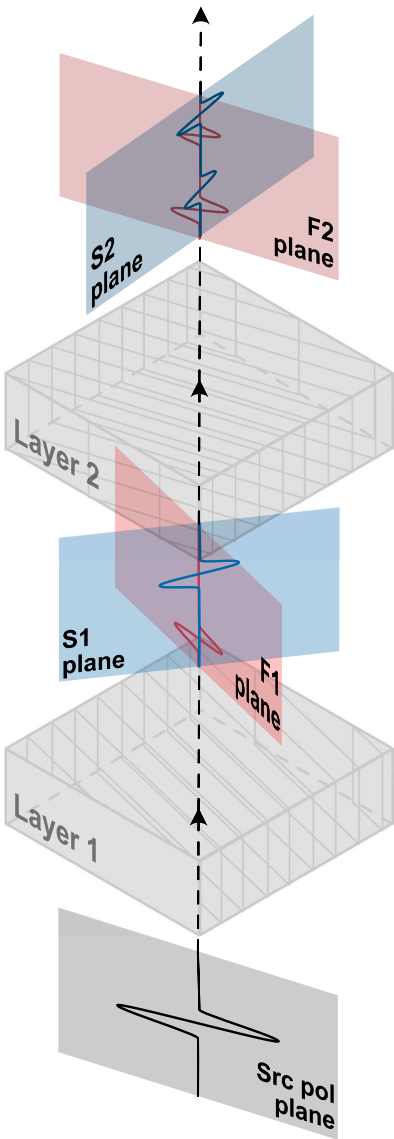

Figure 1 Schematic example of shear-wave splitting through multiple layers with differently oriented fabrics.

cross-correlation (Bowman and Ando, 1987), splitting intensity (Chevrot, 2000), and the eigenvalue method (Walsh et al., 2013; Silver and Chan, 1991; Teanby et al., 2004; Wuestefeld et al., 2010). The method used here for shear-wave splitting analysis is the eigenvalue method (Silver and Chan, 1991; Teanby et al., 2004). Below we describe the exact formulation of the eigenvalue method implemented in SWSPy, first for a single anisotropic layer, before expanding the theory to measure shear-wave splitting for multiple layers of anisotropy.

2.1 The eigenvalue method for a single layer

The eigenvalue method used to measure shear-wave splitting in SWSPy comprises the following steps, for S-wave arrivals at each receiver, for all earthquakes:

1. Load in the data and perform any necessary preprocessing.

2. Rotate data into the LQT (propagation, vertical-transverse, horizontal-transverse) coordinate system.

3. Calculate the ratio of the first and second eigenvlaues (λ_1, λ_2), $\frac{\lambda_2}{\lambda_1}$, for all possible fast directions and delay times

for the optimal splitting parameters ($\delta t, \phi$).

4. Perform clustering analysis to find optimal splitting parameters corresponding to minimum $\frac{\lambda_2}{\lambda_1}$.
5. Calculate the quality measure, Q_W (Wuestefeld et al., 2010), if desired.
6. Calculate the S-wave source polarisation from the shear-wave splitting corrected particle motions.
7. Convert splitting parameter results from LQT to ZNE coordinate system.

2.1.1 Preprocessing

First the data is preprocessed. This involves detrending the data and performing any desired filtering to remove noise while still preserving the S-wave signal. The data can then be upsampled or downsampled, depending upon the native sampling rate and desired computational efficiency. Upsampling the data allows one to resolve δt more precisely, but comes at a computational cost. Upsampling is performed using the weighted average slopes method. Conversely, downsampling decreases the precision of δt measurements but decreases the computational cost by reducing the grid-search over the $\delta t - \phi$ space. Instrument response may also be removed at this stage, which is important if S-wave energy falls outside the constant instrument response band of the instrument.

2.1.2 Rotation into the LQT coordinate system

The three-component (ZNE) data are then converted into the LQT coordinate system (see Figure 2). This requires knowledge of the back-azimuth and incidence angle of the ray at the receiver. Rotating the waveforms into the LQT coordinate system allows shear-wave splitting parameters to be measured in 3D and allows one to trivially use bore-hole as well as surface instruments. Walsh et al. (2013) provide a useful overview of the various coordinate systems that we adopt in this work. SWSPy allows the user to specify to measure splitting in the ZNE coordinate system, which artificially fixes the incidence angle at 0^o from vertical. This assumption is valid for situations where there is a steeply decreasing velocity gradient over multiple wavelengths, typical for the geological setting of most shear-wave splitting studies to date.

2.1.3 Finding optimal splitting parameters

Once the data are rotated, one can perform a grid-search to find the optimal splitting parameters, δt and ϕ, that linearise the data best (energy is maximised in the P-plane and minimised in the A-plane, see Figure 2). This is the splitting method described in Silver and Chan (1991). For each possible δt-ϕ combination, Q(t) and T(t) are rotated by ϕ clockwise in the QT-plane before Q(t) and T(t) are shifted forward and backward in time, respectively, by $\delta t/2$. We then construct a covariance matrix of the Q(t) and T(t) traces and find the eigenvalues of this matrix. The ratio of the first and second eigenvalues (λ_2/λ_1) describes the linearity of the particle motion in the QT-plane, with smaller ratios indicating greater linearity of the data. The ratio $\frac{\lambda_2}{\lambda_1}$ rather than $\frac{\lambda_1}{\lambda_2}$ is used to maximise stability of the solution (Wuestefeld et al., 2010). The δt-ϕ space for an earthquake is shown in Figure 3f. The grid-search is the most computationally intensive step, with the computational cost dependent upon the resolution of both δt and ϕ. To minimise the computational cost, we use the numba compiler (Lam et al., 2015) to wrap the function performing the grid search, allowing it to run as machine code.

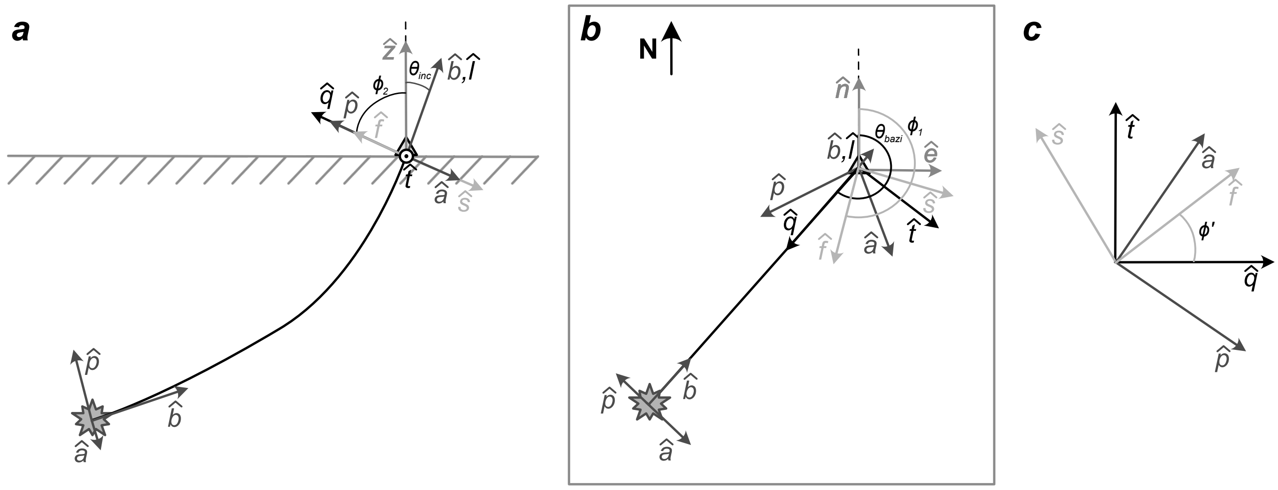

Figure 2 Overview of various coordinate systems. a. LQT and BPA coordinate systems in the vertical plane, with the fast ($\hat{f}$) and slow ($\hat{s}$) directions labelled. b. LQT and BPA coordinate systems in the horizontal plane, with $\hat{f}$ and $\hat{s}$ labelled as before. c. Definition of the various coordinate systems and $\hat{f}$ and $\hat{s}$ in the ray-transverse plane. Various angles are defined as: θ_{inc} is the inclination angle from vertical up of the ray at the receiver; θ_{bazi} is the back-azimuth from North of the ray from the receiver to the source; $\phi_{1,2}$ are the angle of the fast direction relative to North and vertical up, respectively; and ϕ' is the angle of the fast direction from $\hat{q}$.

2.1.4 Multi-window stability clustering analysis

The selection of the start and end of the window around an S-wave phase can significantly affect the stability of the result. In order to find the most stable result, we implement the clustering approach of Teanby et al. (2004), varying the time of the start and end of the windows and clustering the data to find the most stable result. This involves repeating the grid-search in δt-ϕ space for each window. An example of multiple windows can be seen in Figure 3a, with the window duration, start and end window positions, and number of window combinations all possible to specify by the user. The optimal splitting parameters, δt and ϕ, for each individual window are clustered using the DBSCAN algorithm (Ester et al., 1996). This is a deviation from the method of Teanby et al. (2004), since we perform the clustering in a new domain that optimally deals with the cyclic nature of ϕ. The clustering domain, $\mathbf{C}$, is defined by,

$$\mathbf{C} = \begin{pmatrix} \tilde{\delta t}.cos(2\phi) \\ \tilde{\delta t}.sin(2\phi) \end{pmatrix}, \tag{1}$$

where $\tilde{\delta t}$ is the normalised lag time. The optimal overall splitting result for a given source-receiver pair from within all the clusters is defined as the result with the smallest variance within the cluster with the smallest variance, with the within-cluster variance for a given cluster c, $\sigma^2_{cluster,c}$, and the data variance, $\sigma^2_{data,c}$, given by (Teanby et al., 2004),

$$\sigma^2_{cluster,c} = \frac{1}{N_c}\sum_{n=1}^{N_c}(\delta t_n - \bar{\delta t_c})^2 + (\phi_n - \bar{\phi_c})^2, \tag{2}$$

$$\sigma^2_{data,c} = \left(\sum_{n=1}^{N_c}\frac{1}{\sigma^2_{\delta t,n}}\right)^{-1} + \left(\sum_{n=1}^{N_c}\frac{1}{\sigma^2_{\phi,n}}\right)^{-1}, \tag{3}$$

where N_c is the number of samples in cluster c, and $\bar{\delta t}_c$, $\bar{\phi}_c$ are the mean values of δt, ϕ, for cluster c respectively (see Teanby et al. (2004) for further details).

2.1.5 Automation for many receivers and many earthquakes

The clustering method of Teanby et al. (2004) results in stable shear-wave splitting results for a given source-receiver pair, using the eigenvalue method of Silver and Chan (1991). However, typically seismicity studies comprise of tens to hundreds of receivers and catalogues of thousands to hundreds of thousands of earthquakes. A means of automatically quantifying the quality of shear-wave splitting results is therefore desirable. SWSPy contains a class to automatically calculate splitting measurements over entire earthquake catalogues. Three metrics for quantifying the quality of a splitting measurement are: (1) the uncertainty in δt and ϕ, $\alpha_{\delta t}$ and α_{ϕ}, respectively; (2) the linearity of the result, $\frac{\lambda_2}{\lambda_1}$, with smaller $\frac{\lambda_2}{\lambda_1}$ values corresponding to a better result; and (3) the Wuestefeld quality factor, Q_W, which is a measure of the level of agreement between a splitting measurement obtained using the eigenvalue method and the cross-correlation method (Wuestefeld et al., 2010). The cross-correlation method involves cross-correlating the rotated and time-shifted Q and T traces, searching for a maximum similarity between the two waveforms (Wuestefeld et al., 2010). Q_W is given by,

$$Q_W = \begin{cases} -(1 - d_{null}) & \text{for } d_{null} < d_{good} \\ (1 - d_{good}) & \text{for } d_{null} \geq d_{good} \end{cases} \tag{4}$$

where d_{null} and d_{good} are given by,

$$d_{null} = \sqrt{2}\sqrt{\Delta^2 + (\Omega - 1)^2}, \tag{5}$$

$$d_{good} = \sqrt{2}\sqrt{(\Delta - 1)^2 + \Omega^2}, \tag{6}$$

where $\Delta = \delta t_{XC}/\delta t_{EV}$ and $\Omega = (\phi_{EV} - \phi_{XC})/(\pi/4)$. A good measurement with perfect agreement between the eigenvalue and cross-correlation methods should have $\delta t_{EV} = \delta t_{XC}$ and $\phi_{EV} = \phi_{XC}$ ($\Delta = 1, \Omega = 0$), giving $Q_W = 1$, whereas a good null measurement would have $\Delta = 0, \Omega = 1$, giving $Q_W = -1$. Q_W will be near-zero for a poor measurement (see Wuestefeld et al. (2010) for more details). Together, these metrics can be used to identify reliable good and good-null shear-wave splitting measurements in a fully automated way. An example of this is shown in Section 3.3.

2.1.6 S-wave source polarisation

Once an optimal shear-wave splitting result has been obtained, one can remove the effect of shear-wave splitting to retrieve the original S-wave radiated from the earthquake source. The initial S-wave source polarisation can be obtained from the eigenvalues of the anisotropy-removed S-wave particle motions in the QT-plane. The S-wave source polarisation is a useful, yet underused, parameter for seismic analysis since for a double-couple earthquake source, it is the direction of fault slip. We provide an example of how diagnostic source polarisation can be in Section 3.3.

2.1.7 Rotation from the LQT to ZNE coordinate system

Finally, all the results, including the optimal fast direction (ϕ), the various quality metrics, and the S-wave source polarisation are converted from the LQT coordinate system to the ZNE coordinate system (see Figure 2 for definitions of all the relevant angles). The results therefore represent a full 3D result.

2.2 Expanding the method to multi-layer media

The above method has so far only considered the presence of a single anisotropic layer. However, in reality many situations likely exhibit multiple anisotropic layers, potentially with different fast-directions and strengths of anisotropy. Examples might include SKS phases travelling through a mantle layer and a crustal layer (Barruol and Mainprice, 1993), or S-waves originating at the base of an ice stream travelling through a flow-dominated anisotropic layer near the bed and a vertical compressional layer at shallower depths (Kufner et al., 2023). Approximating such systems using a single layer shear-wave splitting method will only allow one to measure the apparent splitting (Silver and Savage, 1994). Obviously this measurement limits the detail to which one can resolve the medium, but it will also result in corrected S-wave arrivals that are not optimally linearised. A multi-layer shear-wave splitting method is thus required to fully describe such systems, providing additional information on the media and optimally linearising the data.

Here, we will refer to measuring shear-wave splitting for two-layers and n-layers somewhat interchangeably. Everything we describe here for a two-layer problem is theoretically possible for $n > 2$ layers, but in practice it is rare that real-world observations would allow for accurate inversion of more than two layers.

Others have developed formulations for solving the multi-layer problem by inverting for two layers simultaneously (Özalaybey and Savage, 1994; Wolfe and Silver, 1998). Although evidence of the performance of these methods is limited by the availability of sufficient quality observations, the methods hold theoretically. However, inverting for two layers simultaneously doubles the number of degrees of freedom, which inevitably leads to a more poorly constrained result. Furthermore, it is highly computationally expensive, with the grid-search space increasing as a power of n-layers ($t_{compute}$ is $\mathcal{O}((n_{angles} \times n_{time-shifts})^{n_{layers}})$). Another method involves splitting the medium a number of box-shaped domains (typically horizontal layers), each with a full anisotropic elastic tensor, and solving the Christoffel equation to find the theoretical splitting parameters (Wookey, 2012; Hammond et al., 2014). These modelled splitting parameters can then be used in combination with observations to form an inversion to find the optimal splitting parameters for each layer. This method is likely more stable than the aforementioned simultaneous method, but requires one to explicitly specify the thickness of anisotropic layers (Wookey, 2012; Hammond et al., 2014; Kufner et al., 2023). The new method we present here, which is incorporated into SWSPy, differs from the aforementioned methods in that we measure and remove the multiple anisotropic layers individually, iterating from the shallowest (or final) layer consecutively to the deepest (or first) layer. This method is limited by the criteria that have to be fulfilled in order to enable measurement of multi-layer splitting compared to the simultaneous method of Özalaybey and Savage (1994) and Wolfe and Silver (1998), but provides better constraint of the result because it doesn't increase the number of degrees of freedom when finding the optimal splitting parameters for each layer. Furthermore, it is significantly more computationally efficient than simultaneous inversion methods, instead scaling as $t_{compute}$ is $\mathcal{O}((n_{angles} \times n_{time-shifts}) \times n_{layers})$. Below we describe the new layer-by-layer method for two layers, the assumptions required, and an extended derivation for n-layers.

2.2.1 Required assumptions

The layer-by-layer method requires a number of assumptions:

1. n layers split the S-wave n times (Yardley and Crampin, 1991; Silver and Savage, 1994).

2. Each layer has a single effective anisotropy. In other words, this method will only resolve the overall effect of all anisotropic contributions within a given layer, in the same way as the single-layer method.

3. The delay-time of the deepest layer (layer-1), δt_1, must be greater than the longest dominant period component of the S-wave.

4. The signal dominating an initial apparent single-layer measurement is that of the first layer of splitting. This constraint is likely valid for the majority of scenarios because the first-layer only partitions the energy between two phases (fast and slow, layer-1).

5. The anisotropy of each layer has the same frequency-dependent behaviour (i.e. S-waves are not differentially dispersed by the various layers).

6. The fast directions of each layer (ϕ_1, ϕ_2, ..., ϕ_n) are not parallel or orthogonal to one another in the QT-plane. If they are orthogonal then it will not be possible to differentiate between phases from the two layers as the fast and slow waves will not undergo further splitting, giving a null result for one of the layers (a null result is defined as where anisotropy is indistinguishable).

Although these criteria might appear stringent, it is likely that a number of physical scenarios meet these conditions.

2.2.2 The method for two-layers

The multi-layer splitting method measures the splitting parameters for each individual layer ($\phi_i, \delta t_i$), as well as the apparent splitting parameters using the single-layer method ($\phi_{app}, \delta t_{app}$) so that the significance of the multi-layer result beyond the single-layer result can be quantified. These parameters are measured as follows:

1. The apparent splitting parameters are measured using the single-layer method for a window, win_{init}, containing all the S-wave energy (see Section 2.1).

2. The initial window is partitioned into two windows, one from $t_{win_{init},start}$ to $t_{win_{init},start} + \delta t_{app}$, and another from $t_{win_{init},start} + \delta t_{app}$ to $t_{win_{init},end}$.

3. The splitting parameters are measured for each of the these windows, using the eigenvalue method (see Section 2.1), with the most linearised result (smallest λ_2/λ_1) defined as the optimal splitting parameters for the shallowest layer (layer 2 for a two-layer problem).

4. The entire S-wave arrival over win_{init} is then corrected to remove the splitting for layer 2.

5. The splitting parameters are then measured for this corrected data over win_{init}. The optimal splitting parameters measured here correspond to the deepest layer (layer 1).

6. One can then confirm whether the two-layer solution provides a more accurate description of the medium than the single-layer, apparent solution. Here, we define this as a solution where the multi-layer result is: (1) more linear (i.e. $(\lambda_2/\lambda_1)_{multi-layer} < (\lambda_2/\lambda_1)_{single-layer}$); and (2) the fast directions of the two layers have different orientations, after accounting for uncertainty. Here, we define $(\lambda_2/\lambda_1)_{multi-layer}$ in a similar way to Wolfe and Silver (1998), except summing over λ_2/λ_1 rather than λ_2,

$$(\lambda_2/\lambda_1)_{multi-layer} = \sum_{n=1}^{n} \left(\frac{\lambda_2}{\lambda_1}\right)_n , \quad (7)$$

where n denotes the nth layer.

2.2.3 Extension to n-layers

Section 2.2.2 describes the multi-layer method specifically for two layers, for clarity. However, extension of the method for n-layers is theoretically trivial. Steps 2 to 4 in Section 2.2.2 can be repeated for cascading smaller windows, using $\delta t_{2,app}, \delta t_{3,app}$, ..., $\delta t_{n,app}$ to partition the windows in each case. However, practically there is a limit to how many layers can be measured independently. Various S-wave phase arrivals are more likely to be indiscernible from one another as the number of layers to solve for becomes greater, since each layer is thinner, which inevitably leads to smaller delay times. Window lengths will also become smaller, leading to less stable solutions. Furthermore, energy partitioning associated with splitting due to each layer will reduce the S-wave amplitudes by $1/2^n$ for n-layers, reducing the SNR of each individual S-wave phase arrival. Therefore, although we include the extension to n-layers for completeness, we only provide examples solving for up to two layers.

2.3 Example of SWSPy usage

SWSPy supports automated measurement of shear-wave splitting for simple single source-receiver pairs to many many receivers and many sources. Here, we provide a simple example of how to measure shear-wave splitting for a single source at multiple receivers and an example of how one can perform forward modelling to generate synthetic signals exhibiting shear-wave splitting. A comprehensive set of examples for every result presented in this work are provided within the SWSPy package.

2.3.1 Measuring shear-wave splitting for an earthquake

SWSPy is implemented using a python class-based structure (see Listing 1), heavily utilising `obspy` for seismic data input and output (Krischer et al., 2015). One creates a `splittingObject`, by passing an `obspy` data stream, `st`, containing seismic traces for all receivers and all components over the earthquake arrival time period. Various parameters defining the windows and parameter search space can then be specified as `splittingObject.parameter`, before performing the shear-wave splitting analysis. The shear-wave splitting analysis in Listing 1 is performed using the function `perform_sws_analysis`, which performs shear-wave splitting for a single layer. To instead use the multi-layer (layer-by-layer) method, one can simply replace this function with the function `perform_sws_analysis_multi_layer`.

Listing 1 Example use of `splittingObject` to perform shear-wave splitting analysis

```
import swspy, obspy

```

```
# Create splitting object:
st = obspy.read(<path_to_data>)
splittingObject = swspy.splitting.create_splitting_object(st)

# Specify some key parameters...
splittingObject.overall_win_start_pre_fast_S_pick = 0.3
splittingObject.overall_win_start_post_fast_S_pick = 0.2
splittingObject.max_t_shift_s = 1.0

# Perform splitting analysis:
splittingObject.perform_sws_analysis(coord_system="ZNE", sws_method="EV")

# Plot and save result:
# (saves splittingObject.sws_result_df to csv file)
splittingObject.plot()
splittingObject.save_result()
```

2.3.2 Forward modelling

SWSPy also supports forward modelling, for generating synthetic seismograms passing through anisotropic media. An example of creating a synthetic seismogram for an S-wave with a dominant frequency of *10 Hz* travelling through a layer that has a fast direction of 60^o and $\delta t = 0.5\ s$ is shown in Listing 2. Such forward modelling is included for verifying SWSPy performance and solving inversion problems, for example.

Listing 2 Example use of generating a synthetic seismogram `st`

```
import swspy

# Create source-time function:
seismogram_dur_s = 10.0
sampling_rate_hz = 1000.0
st = swspy.splitting.forward_model.create_src_time_func(seismogram_dur_s, sampling_rate_hz)

# Specify layer anisotropy parameters:
phi_from_N = 60
dt = 0.5
back_azi = 0
event_inclin_angle_at_station = 0

# Apply splitting:
st = swspy.splitting.forward_model.add_splitting(st, phi_from_N, dt, back_azi,
    event_inclin_angle_at_station)
```

3 Examples

3.1 Simple icequake example

Here, we use a real-world earthquake at a glacier as an example of S-wave splitting analysis performed using SWSPy, specifically focusing on the key attributes that indicate a reliable measurement. Figure 3 shows a basal stick-slip icequake S-wave arrival at a single receiver from Rutford Ice Stream, Antarctica (Hudson et al., 2020a; Smith et al., 2015). Glacier ice can exhibit a strongly anisotropic fabric, which combined with low noise levels in Antarctica provides an ideal real-world example of S-wave splitting (Smith et al., 2017; Harland et al., 2013; Kufner et al., 2023). Basal stick-slip icequakes also provide an ideal example because their S-wave source polarisations are typically well-constrained, aligned approximately in the direction of ice flow (160^o from North (Smith et al., 2015)), in this case confirmed by full-waveform source mechanism inversion (Hudson et al., 2020a).

There are a number of key attributes that represent a well-constrained splitting result. Useful attributes for quantifying the quality of a splitting result are:

1. Checking the raw vs. splitting-removed waveforms in the ZNE coordnate system (see Figure 3a). Firstly, the majority of the S-wave arrival wave packet should lie between the last of the possible window starts and the first of the possible window ends (grey vertical lines, Figure 3a). Secondly, the wave packet of the splitting-removed wave packet have a shorter duration than the raw data.

2. Maximising and minimising energy on splitting-removed P and A components, respectively (red data, Figure 3b). The amplitude ratio of the P to A components represents the linearity of the splitting-removed particle motions, which is quantified by the ratio of eigenvalues (λ_2/λ_1), with smaller λ_2/λ_1 values representing a more linearised result. For the icequake, $\lambda_2/\lambda_1 = 0.033$, with the majority of energy contained in the P component, with only a small packet of energy arriving on the A component.

3. Fast and slow S-wave phases should arrive at different times prior to splitting removal and aligned in time post the removal of splitting (see right panel of Figure 3c).

4. Approximately linear particle motion in the North-East plane (see Figure 3d). For the icequake in Figure 3, the particle motion is approximately linearised, except for a small perturbation approximately perpendicular to the dominant strike, with a source polarisation of $\sim 165^o \pm 6^o$ from North, which is in agreement with the ice flow direction and source mechanism inversion (Hudson et al., 2020a).

5. Checking the stability of the clustering analysis (see Figure 3e). At least some of the cluster samples should have small uncertainties, resulting in a stable ϕ and δt solution. A comprehensive description of how the clustering analysis should be interpreted can be found in Teanby et al. (2004).

6. A distinct minimum in the eigenvalue ratio within $\phi - \delta t$ space (see Figure 3f). The icequake exhibits a distinct, single global minimum, with the optimal solution indicated by the green point and associated error bars. Note that ϕ is ϕ from Q (ϕ', Figure 2). The $\phi - \delta t$ space plot is useful for interrogating whether cycle skipping occurs. If cycle skipping were dominating the result, then there might be multiple minima, with associated ϕ values

separated by 90^o and multiple possible δt values, corresponding to the phase-lag of the cycle skipping. The icequake result shown here is a relatively simple arrival, not exhibiting any significant cycle skipping.

7. Measurement quality parameters λ_2/λ_1 and Q_W. SWSPy outputs multiple parameters that indicate the quality of a S-wave splitting result. The linearity of the result is quantified by the eigenvalue ratio λ_2/λ_1, as discussed above. SWSPy can also calculate the so-called Wuestefeld quality factor, Q_W (Wuestefeld et al., 2010), where $Q_W = 1$ is a good result, $Q_W = 0$ is a poor result, and $Q_W = -1$ is a good null result. Q_W for the icequake in Figure 3 is 0.969, which confirms that the result is consistent using both eigenvalue and cross-correlation methods. However, these measurement quality parameters inevitably are important for automated filtering of many results, for which it is otherwise impractical to check every individual result. For automated analysis, we recommend using quality parameters in combination with uncertainty in ϕ and δt to filter out spurious results (see Section 3.3 for an example).

3.2 Teleseismic shear-wave splitting

Here, we demonstrate the performance of SWSPy for teleseismic shear-wave splitting. Teleseismic shear-wave splitting of SKS, PKS, and SKKS phases is a common technique used to constrain upper mantle deformation patterns (Silver and Chan, 1991; Kendall et al., 2005; Becker and Lebedev, 2021, e.g.). These core transiting phases enable reliable shear-wave splitting measurements of the mantle, due to their near-vertical incidence and radial polarisation caused by a P-to-S conversion when exiting the core (Hall et al., 2004).

Figure 4 shows data from the $M_w 7.1$ 5$^{\text{th}}$ February 2005 Celebus Sea earthquake, recorded at the station NEE in California, US. Previous shear-wave splitting analysis, using the shear-wave splitting code SHEBA (Wuestefeld et al., 2010), identified discrepant SKS-SKKS shear-wave splitting where SKS was a null result (i.e., no shear-wave splitting) and SKKS exhibited clear shear-wave splitting, with $\phi = 74^o \pm 5^o$, $\delta t = 1.05 \pm 0.07s$, which is interpreted as a single layer of seismic anisotropy in the lowermost mantle (Asplet et al., 2020). Unlike the ice example, for teleseismic shear-waves $\delta t << T$, the dominant period of the signal, so the fast and slow S-wave arrivals will not be isolated in time and gives the characteristic elliptical particle motion (see Figure 4d). Using SWSPy, we remeasure the shear-wave splitting of the SKKS phase and obtain $\phi = 74.2^o \pm 14.0^o$, $\delta t = 1.05 \pm 0.175s$ (see Figure 4). These shear-wave splitting parameters agree, within measurement uncertainty, with the SHEBA results. We are also able to retrieve a source polarisation of $115^o \pm 7^o$, which is consistent with the measurement from SHEBA of 115° and the observed back-azimuth of 294^o, following the assumption that SKS is radially polarised. When we correct for the measured shear-wave splitting (see Figure 4d) we can see the particle motion has been well linearised, with $\lambda_2\lambda_1 = 0.018$.

This example only demonstrates a simple teleseismic use case. In reality, modern teleseismic shear-wave splitting studies, particularly those focusing on the lowermost mantle, are more involved. Preprocessing of shear-wave splitting datasets, such as stacking (Deng et al., 2017) and beamforming (Wolf et al., 2023), allow for clearer identification of SKS, SKKS and S3KS phases, especially in noisy datasets. To process large datasets automated approaches for classifying null and split shear-wave splitting using Q_W and λ_2/λ_1 have been developed (Walpole et al., 2014). Advances in modelling plausible anisotropic fabrics from shear-wave splitting measurements (Creasy et al., 2021; Asplet et al., 2023) allow for more quantitative interpretation of observations. The design of SWSPy allows it to be easily integrated

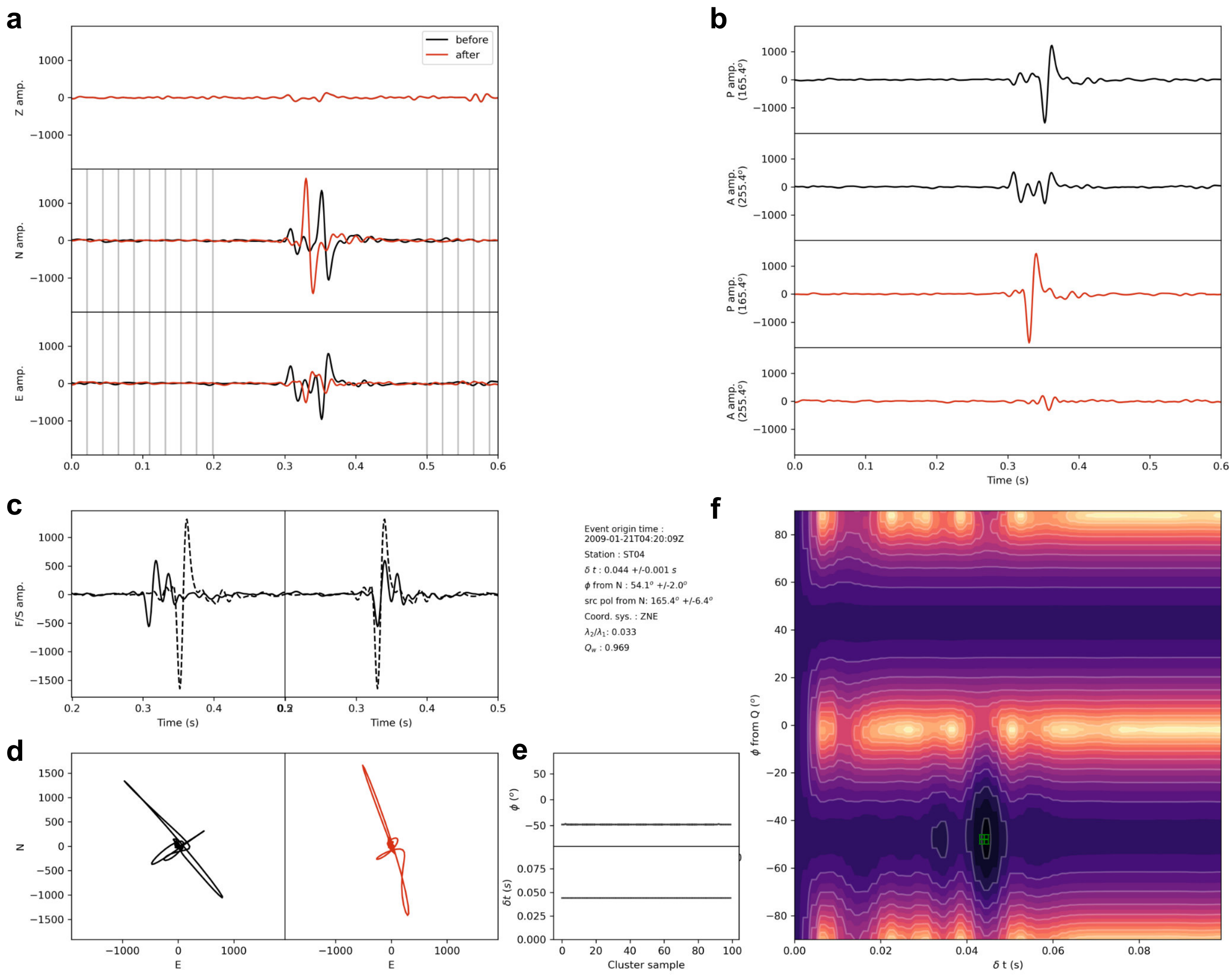

Figure 3 Example of a full output result from SWSPy for an icequake at Rutford Ice Stream, Antarctica, from Hudson et al. (2020a). a. Vertical, North and East component seismograms for the S-wave arrival. Black waveforms are the uncorrected data and red are post splitting correction. b. P and A component waveforms pre and post splitting. c. Fast (solid) and slow (dashed) S-wave arrivals before (left panel) and after (right panel) the delay time shift. d. Particle motions in the North-East plane before (left panel) and after (right panel) the splitting correction. e. Uncertainty in ϕ and δt for all the clustering samples. f. $\phi - \delta t$ space for the optimal cluster result, coloured by eigenvalue ratio. The darker the colour, the smaller the eigenvalue ratio. The optimal splitting result occurs at the global minimum in the $\phi - \delta t$ space, with the optimal solution and its associated uncertainty indicated by the green point and error bars.

into these developing analysis workflows.

3.3 Application of automated S-wave splitting analysis of many earthquakes at a volcano

The previous examples focus on single observations. However, recent advances in the sensitivity and density of instrumentation, combined with computational developments, have resulted in earthquake catalogues containing thousands to millions of events. This presents an opportunity for higher resolution S-wave velocity anisotropy studies. To process such datasets, automation is required. Here, we verify the performance of fully automated S-wave splitting measurements using SWSPy, before showing how this automated S-wave splitting analysis can provide an enhanced picture of the presence of fluids at a volcano.

Results for 1356 earthquakes at Uturuncu volcano, Bolivia, are shown in Figure 5 (Hudson et al., 2023). This earthquake catalogue is derived from a fully automated detection algorithm (Hudson et al., 2022). Figure 5a shows

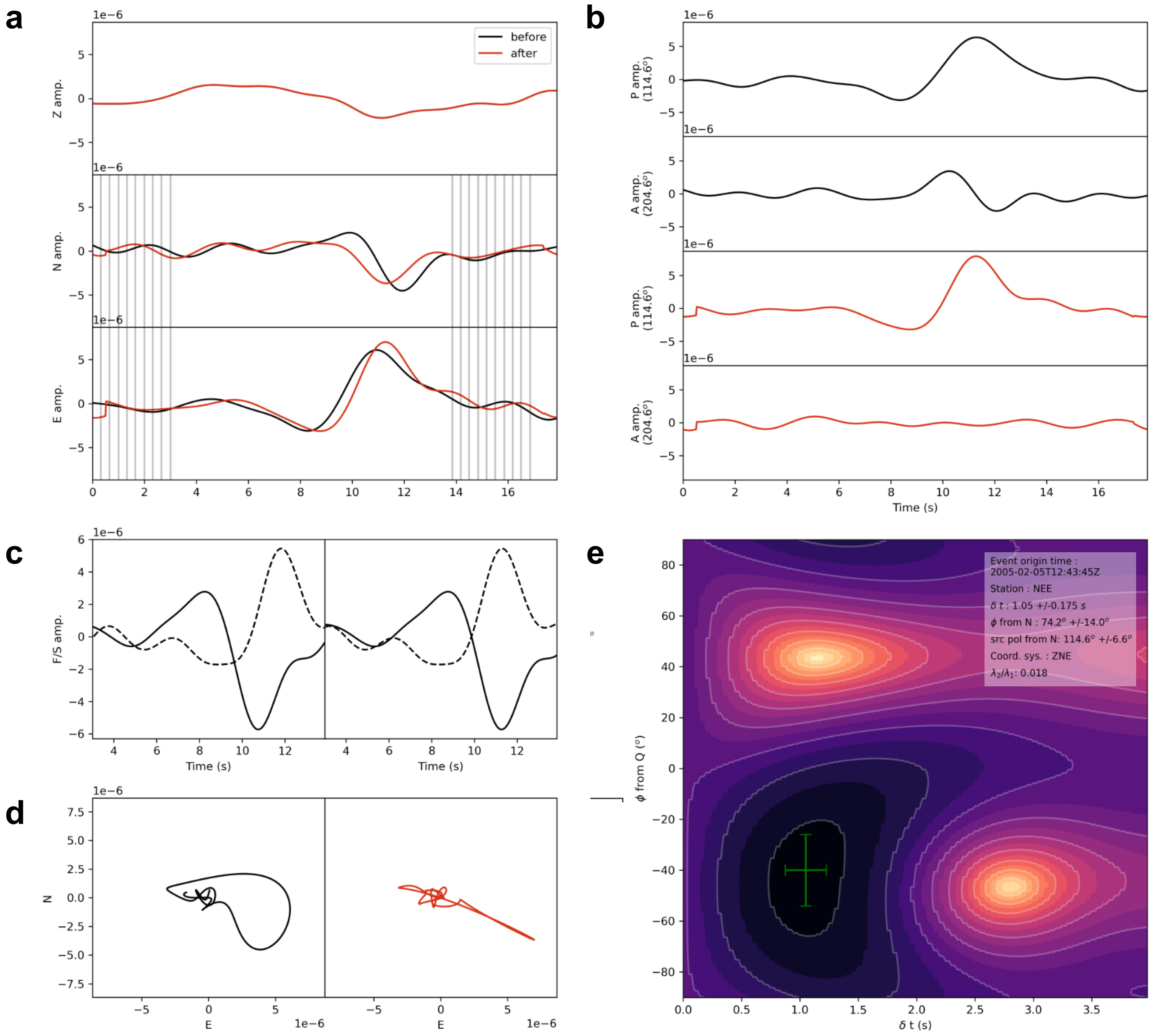

Figure 4 Example of SKKS phase arriving at station NEE from Asplet et al. (2020). a. Vertical, North and East component seismograms for the S-wave arrival. b. P and A component waveforms pre and post splitting. c. Fast and slow S-wave arrivals before and after the delay time shift. d. Particle motions in the North-East plane before and after the splitting correction. e. $\phi - \delta t$ space for the optimal cluster result. See Figure 3 caption for further labelling details.

the unfiltered distribution of fast S-wave polarisations for all source-receiver pairs in the entire Uturuncu dataset compared to a filtered subset of the data. The filtered subset that are defined as well-constrained measurements are S-wave splitting results with $Q_W > 0.5$, a fast S-wave polarisation direction uncertainty, $\alpha_\phi < 10^o$, and a delay-time uncertainty, $\alpha_{\delta t} < 0.1\ s$. The filtered subset of fast directions exhibits one dominant direction of anisotropy striking SE-NW. The anisotropy causing these results could be a combination of the crystallographic orientation of the medium and/or fractures. Here, we assume that for a volcano that is actively deforming (Pritchard et al., 2018), the anisotropy is likely dominated by fracturing (a full discussion of the possible mechanisms of anisotropy and justification of this assumption can be found in Hudson et al. (2023)). To verify whether the measured fast directions shown in Figure 5a are truly representing a fractured fabric, we compare the results to independently measured fault strike data, derived from the spatial distribution of microseismicity (see Hudson et al. (2022) for details). The fault strike data shows two orthogonal sets of fractures (Figure 5b). The fast directions from the shear-wave splitting align parallel to one set of fault strikes. Attenuation tomography at Uturuncu volcano (Hudson et al., 2023) indicates that fluids are likely present dominantly in faults with this orientation, controlled by the regional stress field of the deforming volcano, which is depicted in Figure 5c. The S-wave anisotropy results are therefore consistent with the interpretation from independent observations, verifying the performance of the automated S-wave splitting approach.

The aforementioned filter criteria are necessarily strict, in order to yield sufficiently high quality measurements to interpret. Such strict criteria have limited analysis of automated S-wave splitting measurements in the past because too many events are discarded (Crampin and Gao, 2006). However, recent developments in the number of earthquakes that can be automatically detected means that, in this example, one still has thousands of observations that meet these criteria. This is likely also the case for other datasets. Fully automated shear-wave spliting methods are the only practical means of processing such large datasets.

Shear-wave splitting analysis also yields S-wave source polarisations, which for double-couple faults is oriented in the direction of fault slip. This is clearly illustrated by comparing the fault strikes to SWSPy derived S-wave source polarisations, which approximately agree for both sets of orthogonal fault strikes. The S-wave source polarisations contain a greater spread, either caused by uncertainty in the measurements or by some of the earthquakes exhibiting a volumetric focal mechanism component. However, S-wave source polarisation data are seldom used in anisotropy or crustal-stress studies. We emphasise these observations in order to encourage others to consider using these data to provide additional information on fracture processes and the stress-state of a medium.

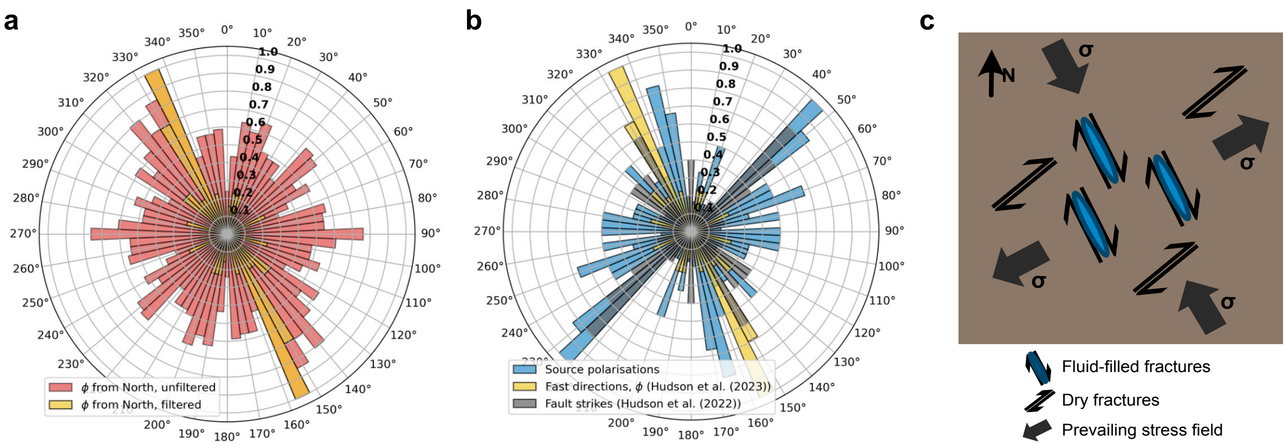

Figure 5 Summary of S-wave splitting analysis for 1356 earthquakes from Uturuncu volcano, Bolivia (Hudson et al., 2023). a. Rose histogram of automatically measured S-wave fast directions, before and after filtering (filters applied are: $Q_W > 0.5$; $\alpha_\phi < 10^o$; $\alpha_{\delta t} < 0.1\ s$). b. Rose histogram of filtered S-wave fast directions, S-wave source polarisations and fault strikes . Fault strikes are derived from principal component analysis of spatial distribution of clustered microseismicity (Hudson et al., 2022). c. Summary of the interpretations of anisotropy combined with source polarisation information.

3.4 Multi-layer examples

3.4.1 Forward model example

We first demonstrate the performance of the new multi-layer splitting method on modelled data, before applying it to a real-world example. Figure 6 shows results for a two-layer forward model. Shear-wave splitting is applied twice to a Ricker wavelet with a centre frequency of *10 Hz* and a source polarisation of $0^o\ N$ to simulate a wave propagating through a two layer medium ($\phi_{layer1} = 60^o$ and $\phi_{layer2} = 40^o$, $\delta t_{layer1} = 0.5\ s$ and $\delta t_{layer2} = 0.2\ s$). Figure 6 show results for an apparent measurement (assuming a single-layer) and our new explicit layer-by-layer approach.

The apparent shear-wave splitting measurement shown in Figure 6a-d obviously does not find the true result. However, the $\phi - \delta t$ space (see Figure 6d) shows that the apparent measurement is sensitive to both layers, with clearly distinct minima at $\delta t = 0.2\ s$ and $\delta t = 0.5\ s$. The first layer exhibits the stronger splitting signal, as expected theoretically, and so is the result that dominates the solution. The sensitivity of this measurement to both layers theoretically makes sense because rotating the original traces into either of the individual layer planes will typically result in more linearised data, but only minimised for one layer. This exemplifies the findings of Silver and Savage (1994), who describe how apparent single-layer splitting measurements can be used to decipher certain aspects of multi-layered anisotropic media. Incidentally, the $\phi - \delta t$ space also shows a strong cycle-skipping signal, caused by the symmetry of the modelled source-time function and the multiple time-shifts resulting from the two layers. It is this cycle-skipping that would make picking the distinct minima for each layer in $\phi - \delta t$ challenging. If this problem could be overcome, then it may be possible in certain instances to isolate relative splitting properties for each layer. Overall, the corrected waveforms are only linearised for layer-2 (see Figure 6c), and the fast-direction and source polarisation are not correct, due to the remaining effect of the layer-1 splitting.

Results for the new layer-by-layer splitting measurement method presented in this work are more promising (see Figure 6i-l). The anisotropy exhibited by the two layers is well resolved by the method, with all results close to the true values and the majority in agreement, within uncertainty. The corrected waveforms further emphasise the performance of our new layer-by-layer method (see Figure 6g compared to Figure 6c). Overall, these results provide us with confidence that our new multi-layer method can resolve multi-layer anisotropy.

3.4.2 Icequake example

There are few real-world examples of successful multi-layer S-wave velocity anisotropy measurements (Silver and Savage, 1994; Rümpker and Silver, 1998; Levin et al., 1999), likely primarily due to challenges associated with making such measurements rather than a lack of real-world multi-layered anisotropic media. However, glacier ice can provide a real-world example of multi-layer anisotropy. Typically, previous glacier anisotropy studies assume a single dominant ice fabric caused by crystals in the ice fabric being preferentially aligned by ice flow (Smith et al., 2017; Harland et al., 2013). However, recent observations suggest that Rutford Ice Stream instead has multiple distinguishable layers of anisotropy (Jordan et al., 2022; Kufner et al., 2023). Indications of this can be seen in Figure 3d, where a proportion of the particle motion in the North-East plane is not fully linearised. We therefore use this icequake to demonstrate performance of the multi-layer splitting method applied to real data.

Figure 7 shows the horizontal particle motion for a two-layer S-wave splitting result compared to the single-layer result from Figure 3. The eigenvalue ratio, λ_2/λ_1, indicates that the two-layer result is approximately twice as well linearised compared to the single-layer result. This demonstrates that a two-layer medium describes the observations better than a single-layer medium. The more linear result also allows for greater constraint of the S-wave source polarisation. The two-layer solution includes the delay-time and fast-direction of both layers. The delay-times of the two layers sum to the delay time measured for a single layer, as expected. The two fast directions are distinct from one another, after accounting for uncertainty. This provides us with confidence that the result represents a physical

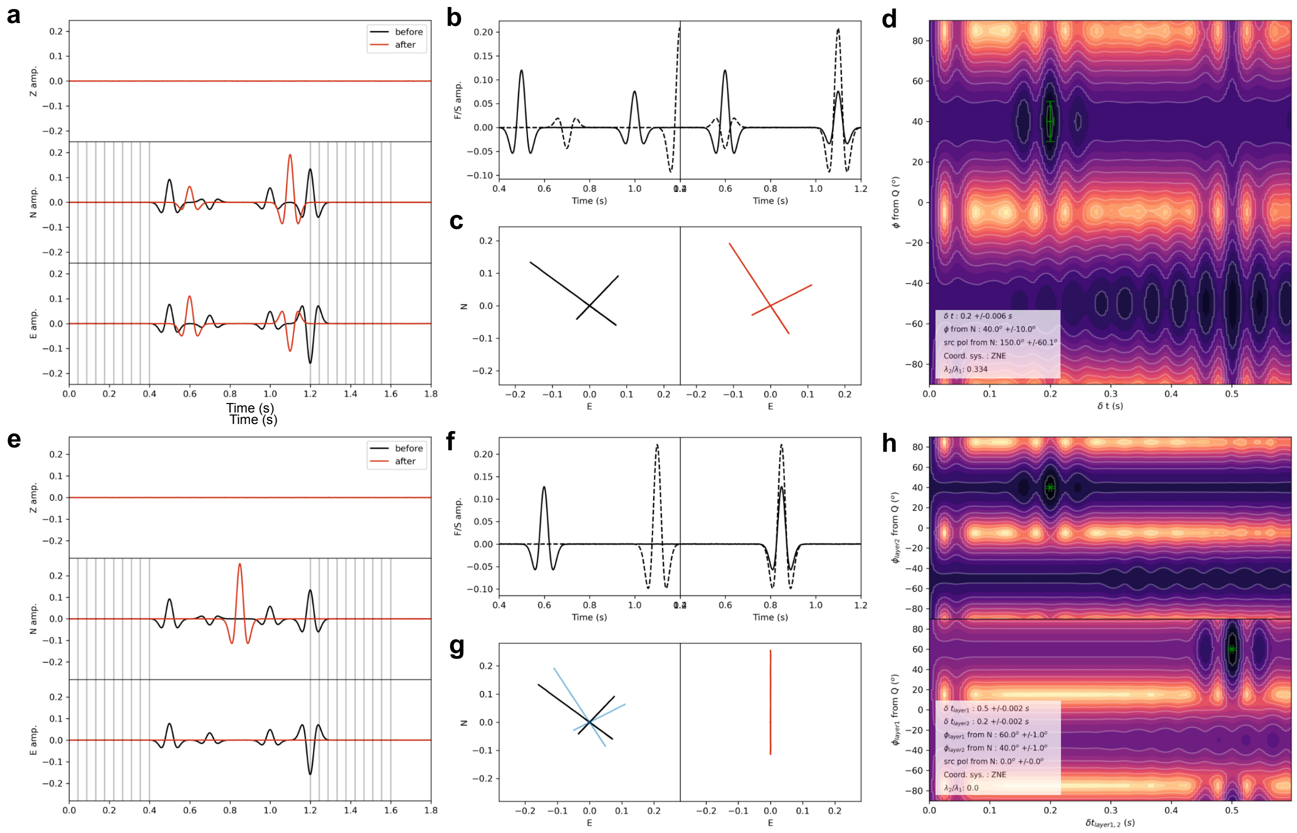

Figure 6 Synthetic, forward model example of multi-layer S-wave splitting analysis, for a medium with two layers of anisotropy ($\phi_{layer1} = 60^o, \phi_{layer2} = 40^o, \delta t_{layer1} = 0.5s, \delta t_{layer2} = 0.2s$) and an S-wave with an initial source polarisation of 0^o from North. (a)-(d). Results for an apparent, effective single-layer measurement (see Figure 3 for more details on labelling of subplots). (e)-(h). Results for an explicit, layer-by-layer two-layer inversion. Blue data in (g)are the particle motions after the intermediate correction for layer-2 only.

two-layer system, rather than a better fit simply being due to an additional two degrees of freedom of the multi-layer solution. However, the additional degrees of freedom of multi-layer splitting analysis should be treated with caution due to the potential for over-fitting. We suggest that one should reject a higher-order layer solution compared to a lower-order layer solution if consecutive layers have fast directions that are the same within uncertainty. This is also why we favour measuring anisotropic layer properties consecutively rather than all together in a direct inversion, as our consecutive-layer method only has the same number of degrees of freedom per layer measurement as the single-layer method.

The icequake result shown in Figure 7 demonstrates that the method shows promise for interrogating multiple layers of anisotropy that are likely present in numerous real-world scenarios.

4 Discussion

4.1 Benefits and limitations

The aforementioned examples indicate the performance of SWSPy for various shear-wave velocity anisotropy applications. For individual source-receiver measurements, it provides stable measurements as a result of the Teanby et al. (2004) multi-window method combined with the use of more advanced clustering algorithms. 3D splitting measurements are implemented, as defined in Walsh et al. (2013), allowing SWSPy to likely be useful for measuring

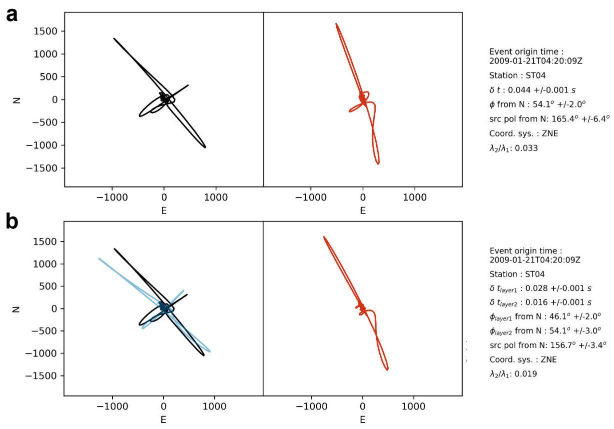

Figure 7 Example of single-layer vs. multi-layer S-wave splitting analysis horizontal particle motions for the icequake in Figure 3. a. Single-layer measurement particle motion results before (left) and after (right) the splitting correction. b. Multi-layer measurement particle motion results before (left) and after (right) the splitting correction (blue data are initial layer-2 only correction). Text in (a) and (b) shows key results from the respective S-wave splitting analyses.

anisotropy using borehole data or settings without a significant shallow velocity gradient. For large datasets comprising of many source-receiver pairs, SWSPy includes a fully-automated workflow that can easily be adapted due to the modular nature of the python package. Parameters that can be used to filter spurious outputs from fully-automated analyses are provided, including quality metrics ($Q_W, \lambda_2/\lambda_1$) and uncertainty measurements ($\alpha_\phi, \alpha_{\delta t}$). The ability to process many thousands to millions of shear-wave splitting measurements will hopefully enable shear-wave velocity anisotropy tomography studies to be performed, with a significant increase in the number of observations reducing the inherently under-constrained nature of the tomography problem. Such anisotropy tomography studies could be useful for imaging deformation at volcanoes (Johnson and Savage, 2012) or measuring fracture density at the surface of glaciers (Hudson et al., 2020b; Gajek et al., 2021).

A further advance provided by SWSPy is the ability to measure multi-layer anisotropy. This will enable users to study systems in more detail, as well as attempt to isolate specific layers of interest. One such example is removing the effect of crustal anisotropy from teleseismic measurements for example, which occurs when the crust and upper mantle have different anisotropic properties (e.g., Silver and Savage, 1994; Hammond et al., 2014; Gao et al., 2010). Multi-layer anisotropy measurements can also be used to discriminate multiple anisotropic layers in the mid (e.g., Wookey et al., 2002; Foley and Long, 2011; Nowacki et al., 2015) or lowermost mantle (e.g., Reiss et al., 2019; Asplet et al., 2020; Lutz et al., 2020). Furthermore, multi-layer measurements could also provide additional observational constraint for anisotropy tomography (Kufner et al., 2023).

SWSPy also has limitations. One limitation is the metrics provided to quantify the quality of a result ($Q_W, \lambda_2/\lambda_1$). While these parameters can prove useful in some instances, we find that they are not universally reliable. We find that the uncertainty measurements provide the most useful way to remove spurious results, at least for the volcanic example provided here (see Figure 5). However, in some cases the stated uncertainty may be an underestimate of the true uncertainty. Areas of further work are therefore better measurement quality metrics and more robustly estimated uncertainty. A further limitation is associated with the layer-by-layer multi-layer anisotropy method presented here. The method requires a specific set of assumptions, and although the data we present here meets these assumptions, it is likely that certain datasets will not. The method should therefore be applied cautiously, considering the assumptions carefully when interpreting any results. A final potential limitation is that SWSPy is written in python, an inherently slow object-oriented language compared to other languages such as C or julia. To minimise this limitation, SWSPy is accelerated using numba (Lam et al., 2015) to compile and parallelise the computationally heavy functions. Although one could further increase the efficiency by implementing the package in a lower level language, we have not opted to do this, in order to make the package as accessible as possible to users.

4.2 Benefits of shear-wave splitting beyond anisotropy studies

The applications of shear-wave splitting reach beyond imaging subsurface anisotropy. A valuable, yet under utilised parameter is the S-wave source polarisation. Figure 5 shows how source polarisation can provide an independent measurement of fault orientation, at least for double-couple sources (Hudson et al., 2023). Another useful output from shear-wave splitting are anisotropy-corrected waveforms. Correcting for anisotropy is important for performing full-waveform inversions using isotropic models, for example to invert for earthquake source mechanisms (Hudson et al., 2020a). The new multi-layer method presented here will further reduce the misfit when comparing data from seismic waves that propagates through multiple anisotropic layers to isotropic full-waveform models. One final application is the removal of shear-wave splitting effects when calculating earthquake magnitudes. Shear-wave splitting can cause S-wave phases to overlap and interfere with one another, altering the apparent frequency content. This can result in additional uncertainty in moment magnitude calculations (Stork et al., 2014). The ability to easily incorporate shear-wave splitting corrections into moment magnitude workflows may reduce uncertainty in moment magnitude catalogues, relevant for improved seismic monitoring (Schultz et al., 2021).

Acknowledgements

T. Hudson was funded by a Leverhulme Early Career Fellowship from the Leverhulme Trust. We thank M. Kendall for useful discussions. We thank all those who collected data used in this study. The data used in this work is all from publicly available sources, and so we direct readers to the cited publications for proper acknowledgement of these individuals.

Data and code availability

The SWSPy package described in this work is available as an open-source python package, hosted on GitHub and PyPi, with a snapshot of the exact version released at time of writing available via Zenodo (Hudson, 2023). All data used in the examples are publicly available and are included as example notebooks within the examples directory of the SWSPy package distribution (Hudson, 2023). The Antarctic icequake data and Uturuncu volcano data are available on IRIS (network codes YG (2009) and XP,YS (2009-2013), respectively), with the data associated with the teleseismic example available from California Institute of Technology and United States Geological Survey Pasadena (1926).

Competing interests

The authors have no competing interests.

References

Asplet, J., Wookey, J., and Kendall, M. A potential post-perovskite province in D beneath the Eastern Pacific: Evidence from new analysis of discrepant SKSa-SKKS shear-wave splitting. *Geophysical Journal International*, 221(3):2075–2090, 2020. doi: 10.1093/GJI/GGAA114.

Asplet, J., Wookey, J., and Kendall, M. Inversion of shear wave waveforms reveal deformation in the lowermost mantle. *Geophysical Journal International*, 232(1):97–114, 2023. doi: 10.1093/gji/ggac328.

Bacon, C. A., Johnson, J., White, R. S., and Rawlinson, N. On the origin of seismic anisotropy in the shallow crust of the Northern Volcanic Zone , Iceland. *JGR Solid Earth*, 2021.

Baird, A. F., Kendall, J. M., Fisher, Q. J., and Budge, J. The Role of Texture, Cracks, and Fractures in Highly Anisotropic Shales. *Journal of Geophysical Research: Solid Earth*, 122(12):10,341–10,351, 2017. doi: 10.1002/2017JB014710.

Barruol, G. and Mainprice, D. A quantitative evaluation of the contribution of crustal rocks to the shear-wave splitting of teleseismic SKS waves. *Physics of the Earth and Planetary Interiors*, 78(3-4):281–300, 1993. doi: 10.1016/0031-9201(93)90161-2.

Becker, T. W. and Lebedev, S. Dynamics of the Upper Mantle in Light of Seismic Anisotropy. In *Geophysical Monograph Series*, pages 257–282. John Wiley Sons, jul 2021. doi: 10.1002/9781119528609.ch10.

Bowman, J. R. and Ando, M. Shear-wave splitting in the upper-mantle wedge above the Tonga subduction zone J. *Geophysical Journal of the Royal Astronomical Society*, 88(March):25–41, 1987.

California Institute of Technology and United States Geological Survey Pasadena. Southern California Seismic Network, 1926.

Chevrot, S. Multichannel analysis of shear wave splitting. *Journal of Geophysical Research: Solid Earth*, 105(B9):21579–21590, 2000. doi: 10.1029/2000jb900199.

Crampin, S. A review of wave motion in anisotropic and cracked elastic-media. *Wave Motion*, 3(4):343–391, 1981. doi: 10.1016/0165-2125(81)90026-3.

Crampin, S. and Chastin, S. A review of shear wave splitting in the crack-critical crust. *Geophysical Journal International*, 155(1):221–240, 2003. doi: 10.1046/j.1365-246X.2003.02037.x.

Crampin, S. and Gao, Y. A review of techniques for measuring shear-wave splitting above small earthquakes. *Physics of the Earth and Planetary Interiors*, 159(1-2):1–14, 2006. doi: 10.1016/j.pepi.2006.06.002.

Creasy, N., Pisconti, A., Long, M. D., and Thomas, C. Modeling of Seismic Anisotropy Observations Reveals Plausible Lowermost Mantle Flow Directions Beneath Siberia. *Geochemistry, Geophysics, Geosystems*, 22(10), 2021. doi: 10.1029/2021gc009924.

Deng, J., Long, M. D., Creasy, N., Wagner, L., Beck, S., Zandt, G., Tavera, H., and Minaya, E. Lowermost mantle anisotropy near the eastern edge of the Pacific LLSVP : constraints from SKS – SKKS splitting intensity measurements. *Geophysical Journal International*, 210(June): 774–786, 2017. doi: 10.1093/gji/ggx190.

Ester, M., Kriegel, H.-P., Sander, J., and Xu, X. A Density-Based Algorithm for Discovering Clusters in Large Spatial Databases with Noise. In *KDD-96 Proceedings*, pages 226–231. Elsevier, 1996.

Foley, B. J. and Long, M. D. Upper and mid-mantle anisotropy beneath the Tonga slab. *Geophysical Research Letters*, 38(2):n/a—-n/a, 2011. doi: 10.1029/2010gl046021.

Gajek, W., Gräff, D., Hellmann, S., Rempel, A. W., and Walter, F. Diurnal expansion and contraction of englacial fracture networks revealed by seismic shear wave splitting. *Communications Earth Environment*, 2(1):1–8, 2021. doi: 10.1038/s43247-021-00279-4.

Gao, S. S., Liu, K. H., and Abdelsalam, M. G. Seismic anisotropy beneath the Afar Depression and adjacent areas: Implications for mantle flow. *Journal of Geophysical Research: Solid Earth*, 115(12):1–15, 2010. doi: 10.1029/2009JB007141.

Hall, S. A., Kendall, J. M., and van der Baan, M. Some comments on the effects of lower-mantle anisotropy on SKS and SKKS phases. *Physics of the Earth and Planetary Interiors*, 146(3-4):469–481, 2004. doi: 10.1016/j.pepi.2004.05.002.

Hammond, J. O., Kendall, J. M., Wookey, J., Stuart, G. W., Keir, D., and Ayele, A. Differentiating flow, melt, or fossil seismic anisotropy beneath Ethiopia. *Geochemistry, Geophysics, Geosystems*, 15(5):1878–1894, 2014. doi: 10.1002/2013GC005185.

Harland, S., Kendall, J.-M., Stuart, G., Lloyd, G., Baird, A., Smith, A., Pritchard, H., and Brisbourne, A. Deformation in Rutford Ice Stream, West Antarctica: measuring shear-wave anisotropy from icequakes. *Annals of Glaciology*, 54(64):105–114, 2013. doi: 10.3189/2013AoG64A033.

Hudson, T. S. SWSPy release 1.0.3. *Zenodo*, 2023. doi: 10.5281/zenodo.8006598.

Hudson, T. S., Brisbourne, A. M., Walter, F., Gräff, D., White, R. S., and Smith, A. M. Icequake Source Mechanisms for Studying Glacial Sliding. *Journal of Geophysical Research: Earth Surface*, 125(11), nov 2020a. doi: 10.1029/2020JF005627.

Hudson, T. S., Brisbourne, A. M., White, R. S., Kendall, J. M., Arthern, R., and Smith, A. M. Breaking the Ice: Identifying Hydraulically Forced Crevassing. *Geophysical Research Letters*, 47(21), nov 2020b. doi: 10.1029/2020GL090597.

Hudson, T. S., Baird, A. F., Kendall, J. M., Kufner, S. K., Brisbourne, A. M., Smith, A. M., Butcher, A., Chalari, A., and Clarke, A. Distributed Acoustic Sensing (DAS) for Natural Microseismicity Studies: A Case Study From Antarctica. *Journal of Geophysical Research: Solid Earth*, 126(7):1–19, 2021. doi: 10.1029/2020jb021493.

Hudson, T. S., Kendall, J. M., Pritchard, M. E., Blundy, J. D., and Gottsmann, J. H. From slab to surface: Earthquake evidence for fluid migration at Uturuncu volcano, Bolivia. *Earth and Planetary Science Letters*, 577:117268, 2022. doi: 10.1016/j.epsl.2021.117268.

Hudson, T. S., Kendall, J. M., Blundy, J. D., Pritchard, M. E., MacQueen, P., Wei, S. S., Gottsmann, J. H., and Lapins, S. Hydrothermal Fluids and Where to Find Them: Using Seismic Attenuation and Anisotropy to Map Fluids Beneath Uturuncu Volcano, Bolivia. *Geophysical Research Letters*, 50(5):1–16, mar 2023. doi: 10.1029/2022GL100974.

Johnson, J. H. and Savage, M. K. Tracking volcanic and geothermal activity in the Tongariro Volcanic Centre, New Zealand, with shear wave splitting tomography. *Journal of Volcanology and Geothermal Research*, 223-224:1–10, 2012. doi: 10.1016/j.jvolgeores.2012.01.017.

Johnson, J. H., Savage, M. K., and Townend, J. Distinguishing between stress-induced and structural anisotropy at Mount Ruapehu volcano, New Zealand. *Journal of Geophysical Research: Solid Earth*, 116(12):1–18, 2011. doi: 10.1029/2011JB008308.

Jordan, T. M., Martín, C., Brisbourne, A. M., Schroeder, D. M., and Smith, A. M. Radar Characterization of Ice Crystal Orientation Fabric and Anisotropic Viscosity Within an Antarctic Ice Stream. *Journal of Geophysical Research: Earth Surface*, 127(6):1–24, 2022. doi: 10.1029/2022JF006673.

Kendall, J. M. Seismic anisotropy in the boundary layers of the mantle. *Geophysical Monograph Series*, 117:133–159, 2000. doi: 10.1029/GM117p0133.

Kendall, J.-M., Stuart, G. W., Ebinger, C. J., Bastow, I. D., and Keir, D. Magma-assisted rifting in Ethiopia. *Nature*, 433(7022):146–148, 2005. doi: 10.1038/nature03161.

Krischer, L., Megies, T., Barsch, R., Beyreuther, M., Lecocq, T., Caudron, C., and Wassermann, J. ObsPy: a bridge for seismology into the scientific Python ecosystem. *Computational Science Discovery*, 8(1):014003, may 2015. doi: 10.1088/1749-4699/8/1/014003.

Kufner, S., Wookey, J., Brisbourne, A. M., Martín, C., Hudson, T. S., Kendall, J. M., and Smith, A. M. Strongly Depth-Dependent Ice Fabric in a Fast-Flowing Antarctic Ice Stream Revealed With Icequake Observations. *Journal of Geophysical Research: Earth Surface*, 128(3):1–25, mar 2023. doi: 10.1029/2022JF006853.

Lam, S. K., Pitrou, A., and Seibert, S. Numba. In *Proceedings of the Second Workshop on the LLVM Compiler Infrastructure in HPC*, pages 1–6, New York, NY, USA, nov 2015. ACM. doi: 10.1145/2833157.2833162.

Levin, V., Menke, W., and Park, J. Shear wave splitting in the Appalachians and the Urals: A case for multilayered anisotropy. *Journal of*

Geophysical Research: Solid Earth, 104(B8):17975–17993, 1999. doi: 10.1029/1999jb900168.

Liptai, N., Gráczer, Z., Szanyi, G., Cloetingh, S. A., Süle, B., Aradi, L. E., Falus, G., Bokelmann, G., Timkó, M., Timár, G., Szabó, C., and Kovács, I. J. Seismic anisotropy in the mantle of a tectonically inverted extensional basin: A shear-wave splitting and mantle xenolith study on the western Carpathian-Pannonian region. *Tectonophysics*, 845(October), 2022. doi: 10.1016/j.tecto.2022.229643.

Lutz, K. A., Long, M. D., Creasy, N., and Deng, J. Seismic anisotropy in the lowermost mantle beneath North America from SKS-SKKS splitting intensity discrepancies. *Physics of the Earth and Planetary Interiors*, 305(January):106504, 2020. doi: 10.1016/j.pepi.2020.106504.

Mroczek, S., Savage, M. K., Hopp, C., and Sewell, S. M. Anisotropy as an indicator for reservoir changes: example from the Rotokawa and Ngatamariki geothermal fields, New Zealand. *Geophysical Journal International*, 220(1):1–17, jan 2020. doi: 10.1093/gji/ggz400.

Nowacki, A., Kendall, J., Wookey, J., and Pemberton, A. Mid-mantle anisotropy in subduction zones and deep water transport. *Geochemistry, Geophysics, Geosystems*, 16(3):764–784, 2015. doi: 10.1002/2014gc005667.

Nowacki, A., Wilks, M., Kendall, J. M., Biggs, J., and Ayele, A. Characterising hydrothermal fluid pathways beneath Aluto volcano, Main Ethiopian Rift, using shear wave splitting. *Journal of Volcanology and Geothermal Research*, 356:331–341, 2018. doi: 10.1016/j.jvolgeores.2018.03.023.

Özalaybey, S. and Savage, M. K. Double-layer anisotropy resolved from S phases. *Geophysical Journal International*, 117(3):653–664, 1994. doi: 10.1111/j.1365-246X.1994.tb02460.x.

Pritchard, M. E., de Silva, S. L., Michelfelder, G., Zandt, G., McNutt, S. R., Gottsmann, J., West, M. E., Blundy, J., Christensen, D. H., Finnegan, N. J., Minaya, E., Sparks, R. S., Sunagua, M., Unsworth, M. J., Alvizuri, C., Comeau, M. J., del Potro, R., Díaz, D., Diez, M., Farrell, A., Henderson, S. T., Jay, J. A., Lopez, T., Legrand, D., Naranjo, J. A., McFarlin, H., Muir, D., Perkins, J. P., Spica, Z., Wilder, A., and Ward, K. M. Synthesis: PLUTONS: Investigating the relationship between pluton growth and volcanism in the Central Andes. *Geosphere*, 14(3): 954–982, 2018. doi: 10.1130/GES01578.1.

Reiss, M. C., Long, M. D., and Creasy, N. Lowermost Mantle Anisotropy Beneath Africa From Differential SKS - SKKS Shear-Wave Splitting. *Journal of Geophysical Research: Solid Earth*, 124(8):8540–8564, 2019. doi: 10.1029/2018jb017160.

Rümpker, G. and Silver, P. G. Apparent shear-wave splitting parameters in the presence of vertically varying anisotropy. *Geophysical Journal International*, 135(3):790–800, 1998. doi: 10.1046/j.1365-246X.1998.00660.x.

Savage, M. K., Wessel, A., Teanby, N. A., and Hurst, A. W. Automatic measurement of shear wave splitting and applications to time varying anisotropy at Mount Ruapehu volcano, New Zealand. *Journal of Geophysical Research: Solid Earth*, 115(12):1–17, 2010. doi: 10.1029/2010JB007722.

Savage, M. S. Seismic anisotropy and mantle deformation: What have we learned from shear wave splitting? *Reviews of Geophysics*, 37(1): 65–106, 1999. doi: 10.1029/98RG02075.

Schultz, R., Beroza, G. C., and Ellsworth, W. L. A risk-based approach for managing hydraulic fracturing–induced seismicity. *Science*, 372 (6541):504–507, 2021. doi: 10.1126/science.abg5451.

Sicilia, D., Montagner, J. P., Cara, M., Stutzmann, E., Debayle, E., Lépine, J. C., Lévêque, J. J., Beucler, E., Sebai, A., Roult, G., Ayele, A., and Sholan, J. M. Upper mantle structure of shear-waves velocities and stratification of anisotropy in the Afar Hotspot region. *Tectonophysics*, 462(1-4):164–177, 2008. doi: 10.1016/j.tecto.2008.02.016.

Silver, P. G. and Chan, W. W. Shear Wave Splitting and Sub continental Mantle Deformation. *Journal of Geophysical Research*, 96:429–454, 1991. doi: 10.1029/91JB00899.

Silver, P. G. and Savage, M. K. The Interpretation of shear-wave splitting parameters in the presence of two anisotropic layers. *Geophysical Journal International*, 5(January):689–691, 1994. doi: 10.1111/j.1365-246x.1994.tb04027.x.

Smith, E., Smith, A., White, R., Brisbourne, A., and Pritchard, H. Mapping the ice-bed interface characteristics of Rutford Ice Stream, West Antarctica, using microseismicity. *Journal of Geophysical Research: Earth Surface*, 120(9):1881–1894, 2015. doi: 10.1002/2015JF003587.

Smith, E. C., Baird, A. F., Kendall, J. M., Martin, C., White, R. S., Brisbourne, A. M., and Smith, A. M. Ice fabric in an Antarctic ice stream interpreted from seismic anisotropy. *Geophysical Research Letters*, 44(8):3710–3718, apr 2017. doi: 10.1002/2016GL072093.

Spingos, I., Kaviris, G., Millas, C., Papadimitriou, P., and Voulgaris, N. Pytheas: An open-source software solution for local shear-wave splitting studies. *Computers and Geosciences*, 134(July 2019):104346, 2020. doi: 10.1016/j.cageo.2019.104346.

Stork, A. L., Verdon, J. P., and Kendall, J. M. The robustness of seismic moment and magnitudes estimated using spectral analysis. *Geophysical Prospecting*, 62(4):862–878, 2014. doi: 10.1111/1365-2478.12134.

Teanby, N. A., Kendall, J., and Baan, M. V. D. Automation of Shear-Wave Splitting Measurements using Cluster Analysis. *Bulletin of the Seismological Society of America*, 94(2):453–463, 2004.

Verdon, J. P. and Kendall, J. M. Detection of multiple fracture sets using observations of shear-wave splitting in microseismic data. *Geophysical Prospecting*, 59(4):593–608, 2011. doi: 10.1111/j.1365-2478.2010.00943.x.

Vinnik, L., Breger, L., and Romanowicz, B. Anisotropic structures at the base of the Earth's mantle. *Nature*, 393(6685):564–567, jun 1998. doi: 10.1038/31208.

Walpole, J., Wookey, J., Masters, G., and Kendall, J. M. A uniformly processed data set of SKS shear wave splitting measurements: A global investigation of upper mantle anisotropy beneath seismic stations. *Geochemistry, Geophysics, Geosystems*, 15(5):1991–2010, 2014. doi: 10.1002/2014gc005278.

Walsh, E., Arnold, R., and Savage, M. K. Silver and Chan revisited. *Journal of Geophysical Research: Solid Earth*, 118(10):5500–5515, 2013. doi: 10.1002/jgrb.50386.

Wolf, J., Long, M. D., Leng, K., and Nissen-Meyer, T. Constraining deep mantle anisotropy with shear wave splitting measurements: challenges and new measurement strategies. *Geophysical Journal International*, 230(1):507–527, 2022. doi: 10.1093/gji/ggac055.

Wolf, J., Frost, D. A., Long, M. D., Garnero, E., Aderoju, A. O., Creasy, N., and Bozdağ, E. Observations of Mantle Seismic Anisotropy Using Array Techniques: Shear-Wave Splitting of Beamformed SmKS Phases. *Journal of Geophysical Research: Solid Earth*, 128(1), 2023. doi: 10.1029/2022jb025556.

Wolfe, C. J. and Silver, P. G. Seismic anisotropy of oceanic upper mantle: Shear wave splitting methodologies and observations. *Journal of Geophysical Research: Solid Earth*, 103(1):749–771, 1998. doi: 10.1029/97jb02023.

Wookey, J. Direct probabilistic inversion of shear wave data for seismic anisotropy. *Geophysical Journal International*, 189(2):1025–1037, 2012. doi: 10.1111/j.1365-246X.2012.05405.x.

Wookey, J. and Kendall, J. M. Constraints on lowermost mantle mineralogy and fabric beneath Siberia from seismic anisotropy. *Earth and Planetary Science Letters*, 275(1-2):32–42, 2008. doi: 10.1016/j.epsl.2008.07.049.

Wookey, J., Kendall, J. M., and Barruol, G. Mid-mantle deformation inferred from seismic anisotropy. *Nature*, 415(6873):777–780, 2002. doi: 10.1038/415777a.

Wuestefeld, A., Al-Harrasi, O., Verdon, J. P., Wookey, J., and Kendall, J. M. A strategy for automated analysis of passive microseismic data to image seismic anisotropy and fracture characteristics. *Geophysical Prospecting*, 58(5):755–773, 2010. doi: 10.1111/j.1365-2478.2010.00891.x.

Yardley, G. S. and Crampin, S. Extensive-dilatancy anisotropy: Relative information in VSPs and reflection surveys. *Geophysical Prospecting*, 39(3):337–355, 1991. doi: 10.1111/j.1365-2478.1991.tb00316.x.